Journal of Petroleum Exploration and Production Technology (2019) 9:51–60
https://doi.org/10.1007/s13202-018-0488-6

ORIGINAL PAPER - PRODUCTION GEOLOGY

# The study of horizontal well excavation technology of point bar during ultra-high water-cut stage based on flow field intensity evaluation

**Guo Qi**[1] · **Wang Xihong**[2] · **Meng Lixin**[1]

Received: 24 October 2017 / Accepted: 10 May 2018 / Published online: 12 June 2018


**Abstract**
The Ming Huazhen group of Gang Dong Oilfield is a medium–high permeability reservoir of meandering stream deposits. It has a high areal and vertical heterogeneity and has entered the stage of extra-high water-cut. Point bar is an important development area for oil sands in meandering stream deposits and the development of a lateral layer is an important factor controlling the distribution of residual oil. The change rule of water displacement in medium–high permeability reservoirs was clearly determined by laboratory experiments. A numerical simulation method was used to determine the time-varying physical properties of the reservoir. Based on the internal configuration of the meandering river point bar, the horizontal well excavation method for residual oil development of point bars during the ultra-high water-cut stage is employed on the basis of the evaluation of flow field intensity. The results show that this method can well reflect the distribution of the flow field in a point bar sand body. The degree of extraction increases by 3.2% if horizontal wells are drilled in the weak flow field rather than in other places.

**Keywords** Medium high permeability reservoir · Ultra-high water-cut stage · Point bar deposit · Internal configuration · Strength of flow field

## Introduction

With the development of oilfields and research on the internal configurations of mean-flow river point bar deposits, exploration of the remaining oil at the ultra-high water-cut stage has become a hot topic. The point bar is affected by the meandering fluvial deposits, and the reservoir is usually distributed in the positive rhythm. In the extra-high water-bearing period, due to the high permeability, high heterogeneity and low degree of consolation, it is easy to form a predominant channel under long-term water flood, which is unfavorable to the production of the site (Sun et al. 2004). Many scholars have studied the laws relating to physical changes in the reservoir during the ultra-high water-cut stage. The development of the superiority channel of the Guan Tao group is 34.7% in the Gu Dao oil field, as determined by an interwell tracer test of 39 Wells (Cui and Zhao 2004).

Because of the long-term erosion due to the injected water, the reservoir properties change, as becomes obvious during the ultra-high water-cut stage (Felsenthal and Gangle 1975). By means of logging interpretation and laboratory core experiments, the change of porosity after water flooding is found to be relatively small, while the variations in the permeability and the phase permeability curve are obvious (Jiang 1997; Jin and Lin 2004). Currently, numerical simulation methods that consider variations in the reservoirs physical properties suffer from defects in terms of reservoir continuity characterization, directional characterization and the stability of the calculation results, and do not take into account the differences between middle porosity middle

✉ Guo Qi
qqqqguoqi@163.com

Wang Xihong
294886756@qq.com

Meng Lixin
294481525@qq.com

[1] Exploration and Development Research Institute, Petro China Da Gang Oilfield, Tianjin 300280, People's Republic of China

[2] Sinopec Shengli Oilfield High Training Center, Shandong 257000, People's Republic of China

permeability reservoirs and high porosity high permeability reservoirs after long-term water flood (Abbaszadeh-Dehghani and Brigham 1983; Dou 2005; Maier and Kocabas 2013). To solve these problems, it is necessary to develop a numerical simulation technique based on experimental research in order to consider the time-varying parameters of the different physical properties.

Many scholars have studied the configuration and residual oil distribution patterns of point bar. Leeder (1973) carried out a study on the relationship between full bank width and full bank depth and deduced the formula for calculating the dip angle of the inner side of the dam. For the first time in river sediments, Allen (1983) clearly defined the three-level interface, which is widely used by many geologists. Jordan and Pryor (1992) found in the study of the modern deposits of the Mississippi compound meander belt that the abandoned channel deposition of the mud fill is the main barrier to the lateral movement of the inner fluid of the river. Zhao (1995), among others, used aerial photographs to describe abandoned channels. The numerical simulation of the conceptual model built by Yue et al. (2007) suggests that the residual oil reserves in the upper part of the river and middle-upper part of the lateral accretionary body are abundant. Combined with the results of modern sedimentation and outcrops, the laterally shales are believed by Zhou et al. (2009) to extend from the upper point to the lower point of the dam and to reach from one-half to two-thirds of the thickness of the reservoir. On the basis of the analysis of the interlayer of the point bar in the Xing Bei area, it is believed by Yan et al. (2014) that the water flood in the lower part of the point bar is serious and the remaining oil is mainly concentrated in the middle-upper part. However, modeling methods for the internal configuration of the point bar and the determination of the horizontal well location in the remaining oil enriched area located in the upper part of point bar during the ultra-high water-cut stage are still in the exploration stage of research.

This study is based on laboratory experiments of medium–high permeability reservoirs that are used to determine the variation rules of the reservoir parameters at different levels during the ultra-high water-cut stage. A three-dimensional geological model of the internal configuration of a point bar is established using interface constraint and multipoint geostatistics. A countermeasure of a horizontal well based on the intensity of the flow field in the high water-cut phase is formed, and this method has been shown to achieve good results in the residual oil excavation of the NmIV-6-3 dam point single sand layer in the second area of the Gang Dong oilfield.

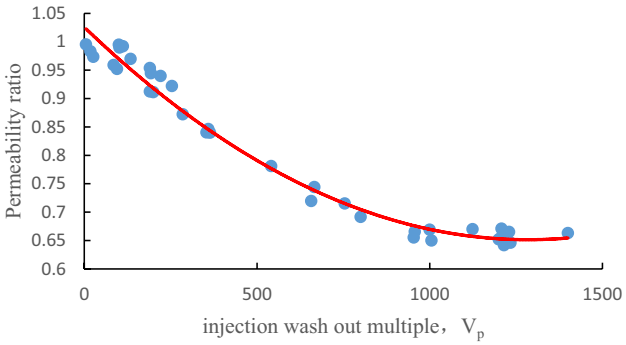


**Fig. 1** Permeability variation with the injection wash out multiple in a middle porosity and middle permeability reservoir

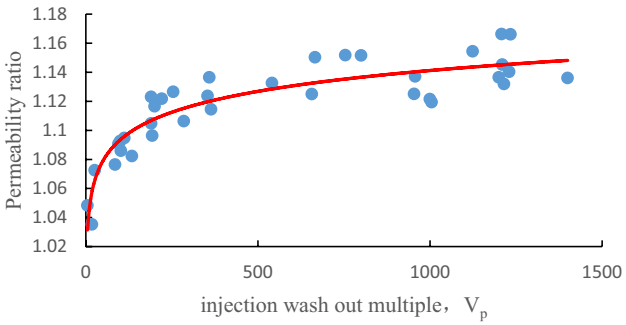


**Fig. 2** Permeability variation with the injection wash out multiple in a high porosity and high permeability reservoir

## The law and characterization method of high water displacement of medium–high permeability reservoirs

The macroscopic properties, microscopic properties and fluid distribution characteristics of a medium–high permeability reservoir in the phase of high water content will change. In order to accurately describe the influence of reservoir parameters on the flow field, a water injection simulation experiment was carried out on a core from the sealing coring well in the Gang Dong block of the Da Gang oilfield and the variation of reservoir parameters was compared at different physical levels.

The physical properties of 58 core samples before and after water flooding were compared and analyzed. Figure 1 shows for the middle permeability of the reservoir. Where the permeability of a core sample is below 500 mD, the correlation of permeability decreases in different degrees and decrease extent decreases in the later development period. However, for high permeability samples with a permeability greater than 1000 mD, with an increase of the injection wash out multiple, the core permeability gradually increases and tends to be stable in the later period, as shown in Fig. 2. The changing trend of water flushing with

the relative permeability of the oil and water in the middle permeability and high permeability reservoirs is such that with an increase of the injection wash out multiple, the residual oil saturation decreases, irreducible water saturation increases (Fig. 3).

For a high permeability reservoir, as the water flood time increases, when the output of the migration particles reach a certain extent, the permeability begin to increase rapidly with the increase of particle output.

The function of the permeability change multiple and the injection wash out multiple are obtained by curve regression.

For a high permeability reservoir:

$$M_k = 0.9966V_p^{0.0195}, \tag{1}$$

For a middle permeability reservoir:

$$M_k = 3 \times 10^{-7}V_p^{2} - 0.0007V_p + 1.0821, \tag{2}$$

where $M_k$ is the permeability change multiple and $V_p$ is the injection wash out multiple.

The function of grid injection wash out multiple and the reservoir properties are used to characterize the variability of the parameters in the ultra-high water-cut stage of a high permeability reservoir. Firstly, the water injection ratio of each grid was deduced according to the Darcy equation. The relationship between the absolute permeability, the relative permeability and the injection wash out multiple was then obtained by analyzing the experimental data. Substituting this relationship into the parametric time-varying mathematical model, the expression for the injection wash out multiple was obtained as follows:

$$R_w(i) = \frac{\int_0^{t_D} Q_{in}\mathrm{d}t}{V_i\emptyset_i}, \tag{3}$$

where $R_w(i)$ is the injection wash out multiple, $i$ is the grid number, $t_D$ is the cumulative injection time, s. $Q_{in}$ is grid water injection rate, $m^3/s$, $V_i$ is the volume of grid $i$, $m^3$, $\varnothing_i$ is the porosity of grid $i$.

A parametric time-varying mathematical model can be established to reflect the characteristic properties of the Gang Dong oil field. In this model, the absolute permeability and relative permeability curves of the reservoir change with the water injection multiple, and the continuity equations of the three phases of oil, water and gas are as follows,

$$\text{Oil component: } \nabla\left[\frac{k(f_w)k_{ro}(f_w,S_w)}{B_o\mu_o}\nabla(p_o-\rho_o gD)\right] + q_{vo} = \frac{\partial}{\partial t}\left(\emptyset\frac{S_o}{B_o}\right), \tag{4}$$

$$\text{Water component}: \nabla\left[\frac{k(f_w)k_{rw}(f_w,S_w)}{B_w\mu_w}\nabla(p_w-\rho_w gD)\right] + q_{vw} = \frac{\partial}{\partial t}\left(\emptyset\frac{S_w}{B_w}\right), \tag{5}$$

$$\text{Gas component}: \nabla\left[\frac{k(f_w)k_{rg}(f_w,S_w)}{B_g\mu_g}\nabla(p_g-\rho_g gD)\right] + \nabla\left[\frac{R_{so}k(f_w)k_{ro}(f_w,S_w)}{B_o\mu_o}\nabla(p_o-\rho_o gD)\right] + \nabla\left[\frac{R_{sw}k(f_w)k_{rw}(f_w,S_w)}{B_w\mu_w}\nabla(p_w-\rho_w gD)\right] + q_{vg} = \frac{\partial}{\partial t}\left[\emptyset\left(\frac{S_g}{B_g}+\frac{R_{so}S_O}{B_o}+\frac{R_{sw}S_w}{B_w}\right)\right], \tag{6}$$

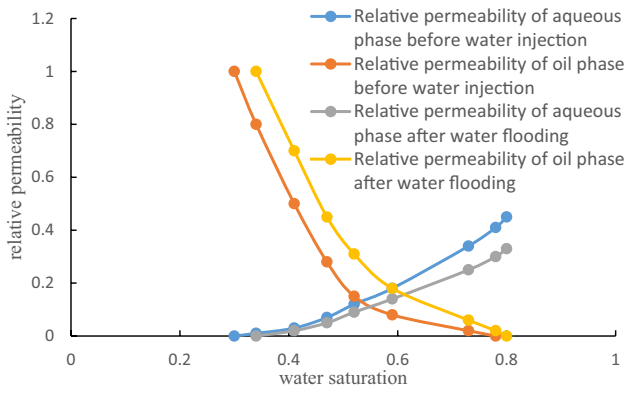


**Fig. 3** Relative permeability curve variation with the injection wash out multiple

where $k$ is the absolute permeability of reservoir; $v_o$, $v_g$, $v_w$ are the flow velocities of the oil phase, gas phase and water phase; $k_{ro}$, $k_{rg}$, $k_{rw}$ are the relative permeabilities of the oil phase, gas phase and water phase; $u_o$, $u_g$, $u_w$ are the viscosities of the oil phase, gas phase and water phase; $p_o$, $p_g$, $p_w$ are the pressures of oil phase, gas phase and water phase; $S_o$, $S_g$, $S_w$ are the saturations of oil phase, gas phase and water phase; $\rho_o$, $\rho_g$, $\rho_w$ are the densities of oil phase, gas phase and water phase; $g$ is the gravitational acceleration; $D$ is the depth calculated from a base surface; $B_o$, $B_g$, $B_w$ are the volumetric factors of the oil phase, gas phase and water phase; $q_o$, $q_g$, $q_w$ are the flow rates in unit volume of rock and unit time of the oil phase, gas phase and water phase; $\varnothing$ is the rock porosity; $R_{so}$ is the solution gas–oil ratio; $q_{vo}$, $q_{vg}$,

$q_{vw}$ are the volume flows rate under standard conditions of the oil phase, gas phase and water phase; $R_{sw}$ is the solution gas–water ratio.

The calculation process is based on the solution of the numerical model whose parameters are time varied based on the IMPES method. In the iteration of each time step the pore volume multiple of the injected water is calculated. Then, on the basis of permeability and relative permeability changing with the injected water flushing pore volume ratio, each grid block permeability and oil water relative permeability value at this time step can be calculated using an interpolation method.

## Determination of the strength evaluation parameters of the flow field during ultra-high water-cut

The main concepts relating to flow field strength assessment are the application of an analytical hierarchy process to determine the parameters which can greatly influence the flow field strength during the ultra-high water-cut stage followed by the formation of unified representation parameters describing the flow field intensity quantitatively. At the same time, economic factors should be considered in order to determine the range of economically recoverable reserves of new wells. Through these two parameters, we can determine the location of the horizontal well of the point bar with the development of the lateral product layer during the ultra-high water-cut stage.

Static factors such as permeability and porosity that affect the intensity of the flow field during the ultra-high water-cut stage in the sedimentary point bar of a meandering river with medium–high permeability are reflected in the geological model and the dynamic parameter changes. For the dynamic parameters of accumulated injection wash out multiple, water saturation, fluid velocity and pressure gradient, the flow velocity can be characterized by the pressure gradient. The injection wash out multiple has a relationship with the water saturation and the fluid flow rate is a reflection of the accumulated injection wash out multiple derivative over time, so the accumulated injection wash out multiple is selected as the index of flow field strength.

Due to the difference between the accumulative injections water multiple in different areas in the late stage of water flooding development, a log function is selected to define the coefficient of flow field strength. After normalizing Eq. (3) results, its expression is,

$$L = \frac{\mathrm{Ln}R_w(i) - \mathrm{Ln}R_w(i)_1}{\mathrm{Ln}R_w(i)_2 - \mathrm{Ln}R_w(i)_1}, \tag{7}$$

where $L$ is the flow field intensity value; $R_w(i)_1$ is the minimum value of the accumulated injection wash out multiple; $R_w(i)_2$ is the maximum value of the accumulated injection wash out multiple.

**Table 1** Standard of flow field intensity division

| Flow field level | Flow intensity value | Name |
|---|---|---|
| 1 | 0.7–1 | Dominant flow zone |
| 2 | 0.4–0.7 | Weak flow zone |
| 3 | 0–0.4 | Non-dominant flow zone |

According to the normalized results, the level of flow field intensity is determined (e.g., Table 1 is about here).

According to the breakeven point method, the remaining economically recoverable reserves of a single well can be determined for which the expression is,

$$I_{pe} = \frac{N_{pe}}{A}, \tag{8}$$

where $I_{pe}$ is the remaining economically recoverable reserves of a single well, 104t/km$^2$; $N_{pe}$ is the remaining economically recoverable reserves, 104$t$; $A$ is a single well controlled area, $m^2$.

The remaining economically recoverable reserves of a single well in Eq. (8) can be calculated according to the following:

$$N_{pe} = \frac{I \times (1+\beta) + t \times C_G}{\alpha_0 \times (P_o - R_T - C_{f-C_o})}, \tag{9}$$

where $\alpha_0$ is the oil or gas commodity rate; $P_o$ is oil and gas sale price; $R_T$ is taxies of per ton oil, Yuan/$t$; $C_f$ is the cost of oil and gas production and operation, $t$ is an evaluation term, years; $C_G$ is the fixed cost of a single well, tens of thousands of Yuan per year; $I$ is the single well development investment, Yuan; $C_o$ is the variable cost per ton of oil, Yuan/$t$; $\beta$ is the coefficient of the well.

The expression for the recoverable reserves of a point bar reservoir is

$$I_o = 100h\phi(S_o - S_{or})\rho_o/B_o \cdot A', \tag{10}$$

where $I_o$is the reservoir recoverable reserves, $10^4$t/km$^2$; $h$ is reservoir thickness, m; $\varphi$is porosity; $S_o$ is oil saturation; $S_{or}$ is residual oil saturation; $\rho_o$ is oil density t/m$^3$; $B_o$ is oil volume factor; $A'$ is the numerical simulation grid area, km$^2$.

When $I_o$is bigger than $I_{pe}$, it is believed that horizontal well excavation is economical and effective. In combination with the flow field strength, horizontal wells can be deployed in the weak point of the flow field during the high water-bearing period, which can result in the effective excavation of the residual oil rich areas caused by the lateral accretion shield of the high water-bearing period.

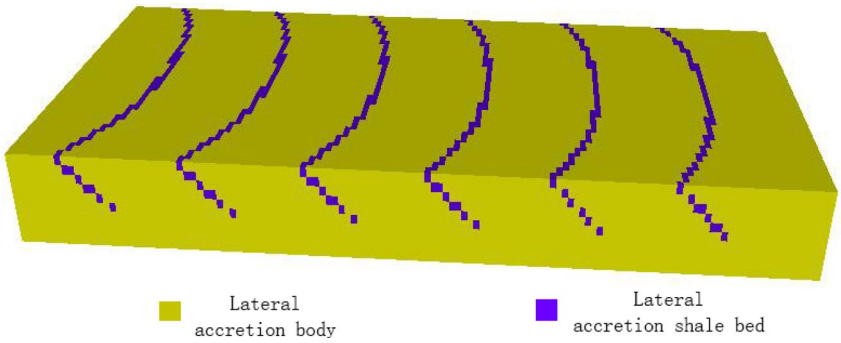


**Fig. 4** Conceptual model of point bar

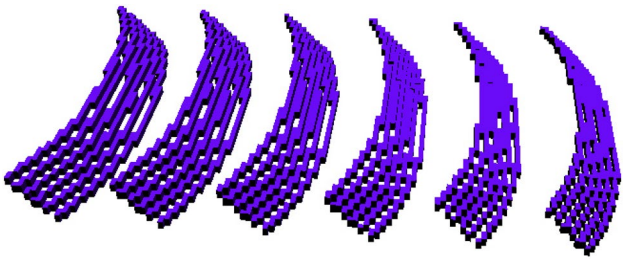

**Fig. 5** The lateral accretion model of point bar

## Study of the method of horizontal well excavation in the ultra-high water-cut stage OG point bar

A model of a meandering river point bar in the Da Gang oilfield is used to illustrate the method of horizontal well excavation. In this model, the horizontal width of a single lateral accretion body is 70 m and the thickness of the sand body is 10 m, as shown in Fig. 4. Figure 5 shows that the average inclination of the lateral accretion layer is 8°.the average thickness of the lateral accretion inter-bed is 1 m and the developed depth of the lateral accretion mudstone accounts for two-thirds of the thickness of the sand body. Based on the interface constraint method (Luchi et al. 2012), a numerical simulation model of the block is established.

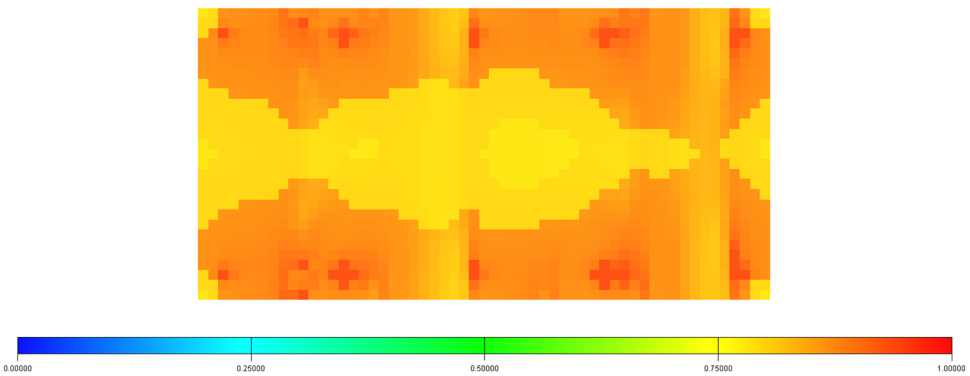


**Fig. 6** Flow field strength distribution at the reservoir bottom without considering parameters as time-varying

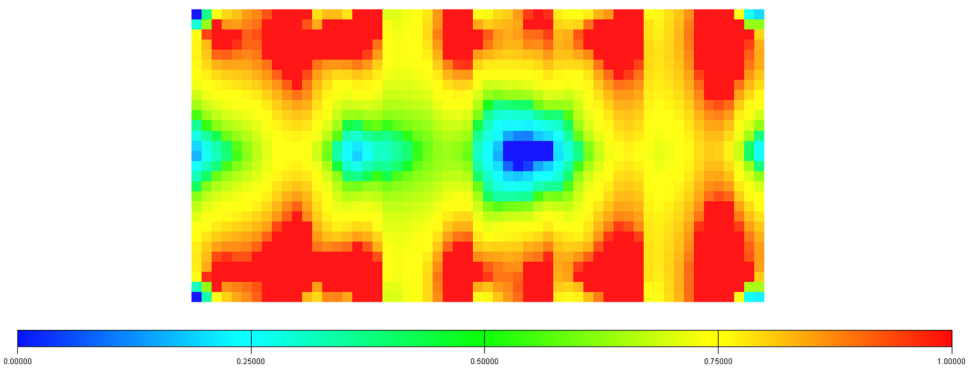


**Fig. 7** Flow field strength distribution at the reservoir bottom considering parameters as time-varying

The permeability of the lateral accretion layer is 1000 mD, porosity is 25%, the longitudinal grid is divided into 10 parts, the fluid and high pressure physical property parameters are derived from the actual data of the reservoir and a four-injection-6 striated pattern is used to produce until the water-bearing rate reaches 98%.

By contrast, the flow field strength distribution at the reservoir bottom shown in Figs. 6 and 7, which represent the cases without and with time-varying parameters, respectively, indicates that the high-intensity flow field in the extra-high water content period is more concentrated in the area between the main line of the oil wells and water wells. Also, the intensity of the flow field at the reservoir bottom is differentiated by the influence of the flow field intensity after long-term water flooding in the bottom of the reservoir because of the influence on of the long-term water flush.

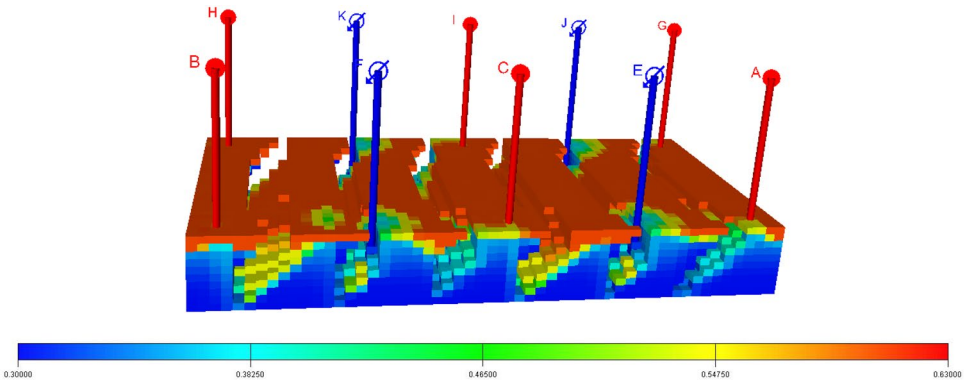


**Fig. 8** The distribution of residual oil in the high water content period in point bar row well pattern

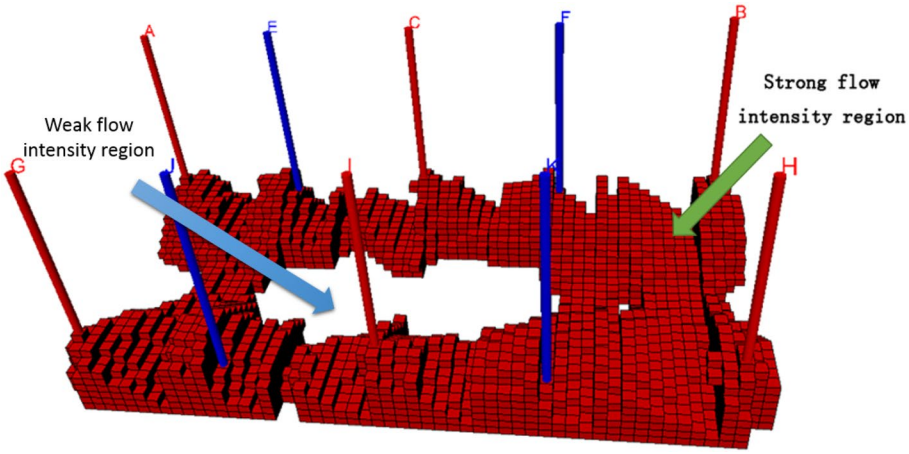


**Fig. 9** Strong flow intensity region

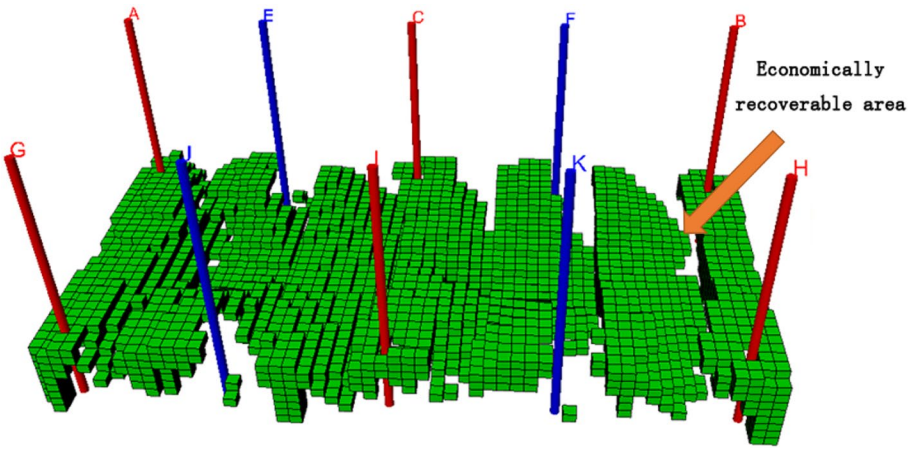


**Fig. 10** Economically recoverable area

Both simulation results show the influence of the lateral accretion shale interlayer and oil accumulation on top of the reservoir, as shown in Fig. 8.

On the basis of considering the changes to the reservoir parameters, the strength of the reservoir (Fig. 9) and the abundance of economically recoverable reserves (Fig. 10) are analyzed. The weak flow field intensity area is shown in the non-well-controlled area in the middle of the reservoir, and the recoverable reserves in the top area of the reservoir are greater than the economic limit of recoverable reserves. Thus the reservoir is suitable for the deployment of horizontal wells.

Considering the strength of the flow field and the evaluation results of the economically recoverable reserves, a reasonable horizontal well spacing should be in the upper part of the weak flow field intensity area. Horizontal wells are deployed in the weak flow field and near the reservoir boundary, and are shown in Fig. 11. In the position of weak flow field strength, the horizontal well was deployed to increase the oil production by 43,000 tons and to decrease the water content by 5.2%. Thus, the effect on development was significantly improved (Fig. 12).

Due to the influence of fluid, formation, well pattern and other factors, the displacement energy imbalance of oil reservoirs can affect their development. The residual oil of point bar during ultra-high water-cut stage is enriched in the upper part and highly dispersed in the lower part. The development effect is obviously better than the development effect of an unbalanced flow field if the well network is adjusted based on the oil reservoir overall flow field strength equilibrium during excavating of the remaining oil enrichment zone located in the upper part of point bar.

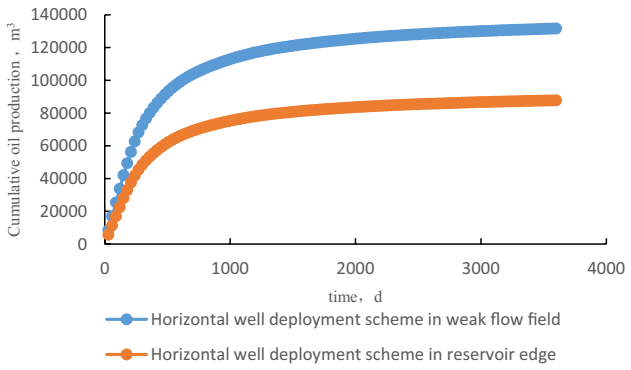


**Fig. 12** Comparison diagram of cumulative oil output in horizontal well deployment

## Application example

Taking the sand layer fault of the second zone of Gang Dong as an example, the actual reservoir geologic model of the internal configuration of a point bar is established using multipoint geostatistics. The block is a typical medium–high permeability reservoir, and the group of Ming Hua town is a meandering river deposit with strong heterogeneity. The oil–water relationship is complicated in the high water content development stage and the water consumption per ton of oil is high with a non-uniform water injection wash out for each area of the oil reservoir.

The internal interlayer of the point bar shows obvious natural potential returns on the logging curve, lower microelectrode log values and the micropotential log is basically coincident with the microgradient curve, as shown in Fig. 13. The method of determining the dip angle of the mudstone interlayer is mainly based on the height difference of the lateral accreted mudstone top of the adjacent wells G7-31 and

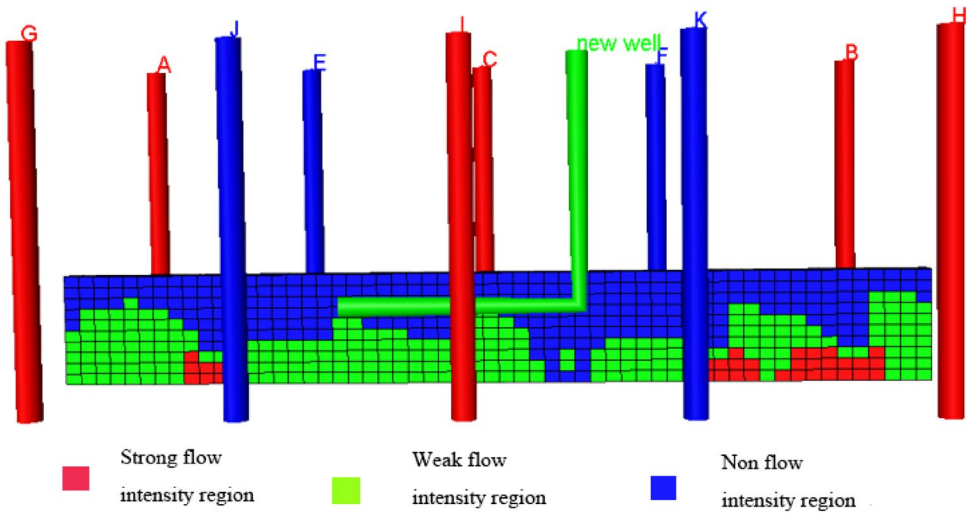


**Fig. 11** Optimal location map of horizontal well excavation in weak flow field

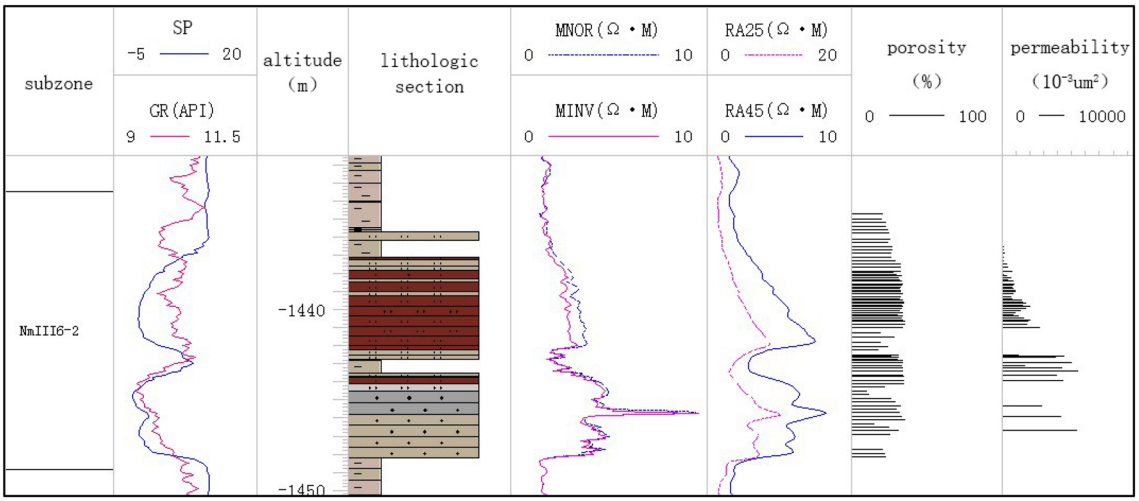


**Fig. 13** Well log response curve of lateral accumulation mudstone in well Gang225

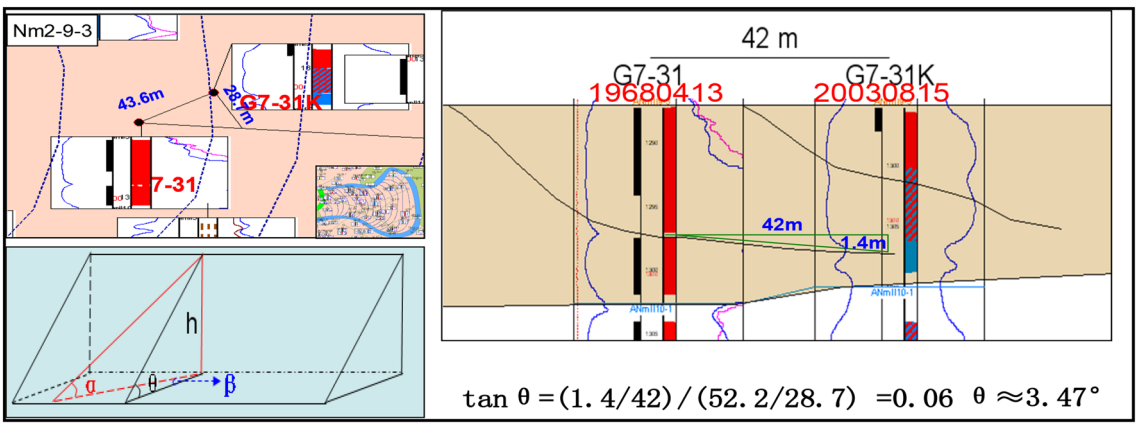


**Fig. 14** Calculation chart of lateral mudstone formation in wells G7-31 and G7-31K

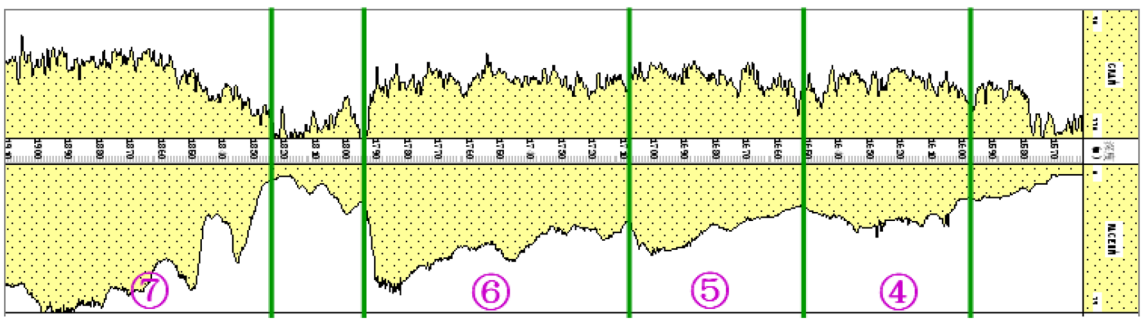


**Fig. 15** The internal configuration of the point bar sand body of Well GH2

G7-31K. The line distance between two wells determines the apparent dip angle of the lateral accretion mudstone. Based on the angle between the direction of the two wells and the true inclination of the lateral mudstone, the tilt angle of the lateral accretion mudstone is estimated to be 3.47° after the coordinate transformation, as shown in Fig. 14.

In the study of the internal configuration of the point bar, the well point with obvious interlayers inside the point bar is the control point. According to the configuration of the channel (abandoned river channel) and point bar, the occurrence, number and size of lateral accretion mudstones are predicted. As shown in Fig. 15, the internal study of the NmIII-6-3 single sand reservoir of GH2 well was studied. According to the assumption of a single sand body structure in the point bar and knowledge of the scale and occurrence of lateral accretion mudstones established in the previous study, the lateral accretion mudstone interlayer identification of well GH2 is carried out to analyze the scale of the body. This study shows that the single sand body is composed of ten imbricate lateral accretion layers with the scale of lateral accretion layers being about 70 m and the development depth of the lateral accrete mudstone is about two-thirds of the thickness of the sand body.

According to the above results, the spatial structure of the geological variables expressed by the variable difference

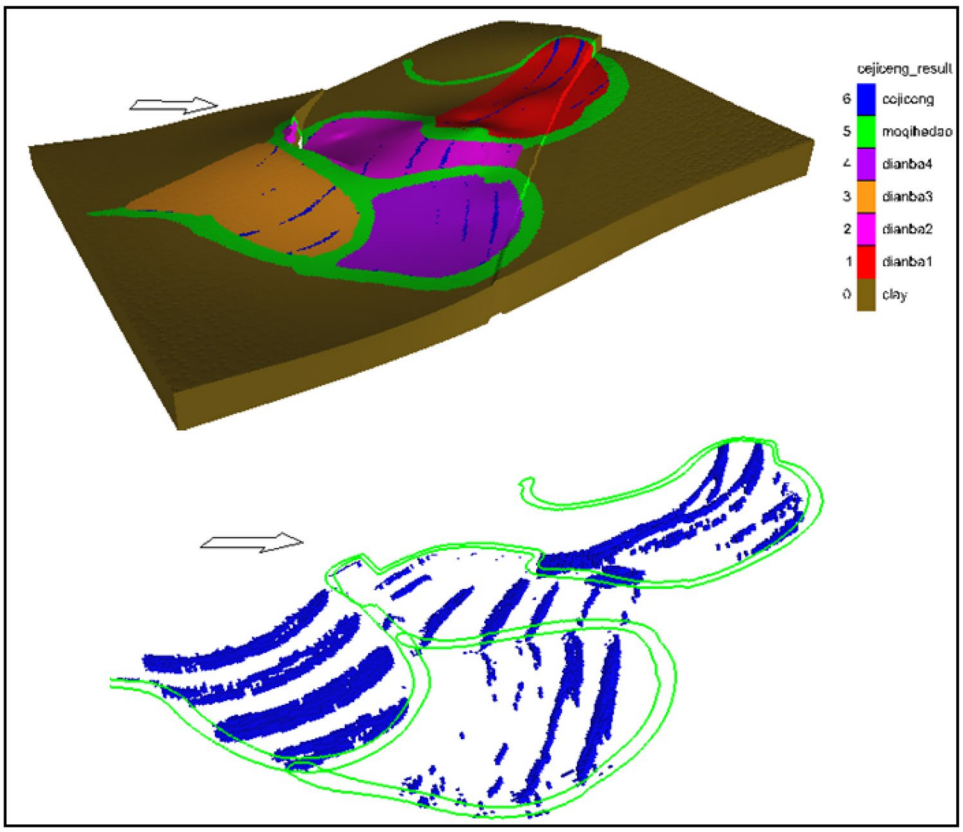


**Fig. 16** Simulated result of the NmIII-3-6-1 point bar interlayer of Gang 3-37 well zone

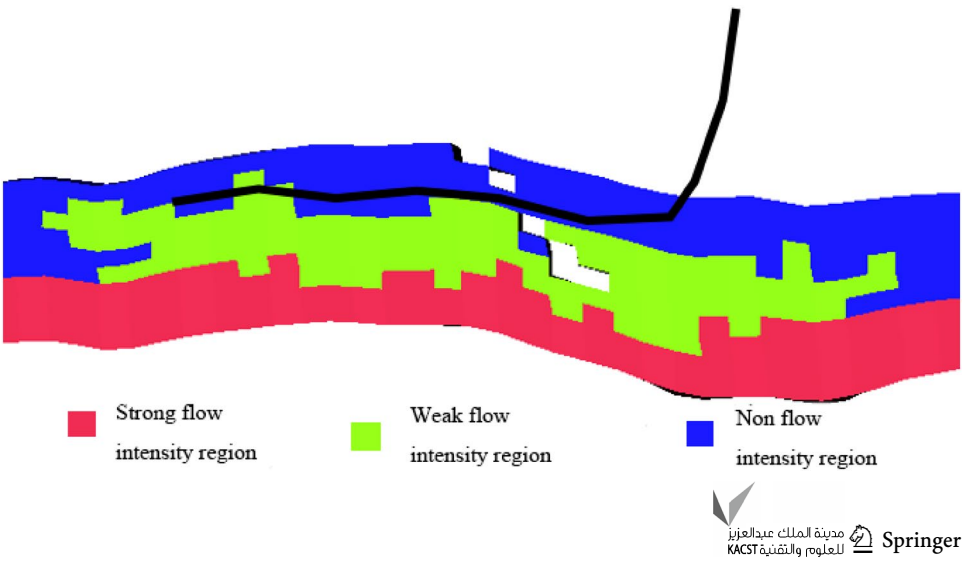


**Fig. 17** Diagram of a new horizontal well based on flow field evaluation

function is replaced by the use of training images in the multipoint geostatistics, which can overcome the problem of the traditional geological statistics not being able to reproduce the deficiencies of the target geometry. The Single Normal Equation Simulation—SNESIM is used to be faithful to the sampling data, with a speed that is better than the random simulation algorithm based on the target. Based on this, the geological model for the internal configuration of the point bar of the Gang Dong oilfield is completed, as shown in Fig. 16.

As shown in Fig. 17, the numerical simulation of the time-varying parameters of a single point bar in the Gang 3-37 well zone was studied, and the intensity of the flow field and economic zone were evaluated. Finally, the location of rational horizontal well excavation is determined. The output of the new horizontal wells is predicted, the output of production is 164,000 tons at the end of the fifteenth year, and the development effect is obviously improved.

## Conclusions

After long-term water injection wash out, the pore throat decreases and the physical properties become worse in middle porosity and middle permeability reservoirs, while the pore throat increases and the physical properties become better in high porosity and high-permeability reservoirs. In the later stage of the extra-high water content development of point bar, the flow field intensity in each region of the reservoir is differentiated because of the influence of the well pattern and relationship between injection and production. The remaining oil shows enrichment in the upper part and dilution in the lower part. The equilibrium of the flow field strength should be considered to adjust the well network when excavating the residual oil enrichment area at the top of the point bar. Based on the flow field strength and the evaluation of the economic limit of residual recoverable reserves, the point bar during ultra-high water-cut stage was evaluated and the position of horizontal well was determined that can guide the remaining oil excavations.

**Acknowledgements** This work was supported by the National Science and Technology Major Project (2017ZX05009001). National Natural Science Foundation of China (51674279). The authors would like to acknowledge the technical support of PETREL and ECLIPSE in this paper.



## References

Abbaszadeh-Dehghani M, Brigham WE (1983) Analysis of unit mobility ratio well-to-well tracer flow to determine reservoir heterogeneity. Am J Clin Nutr 82(4):821–828

Allen JRL (1983) Studies in fluviatile sedimentation. bar complexes and sandstone sheets (lower-sinuosity braided streams) in the Brownstones (L. Devonian), Welsh Borders. Sediment Geol 33:237–293

Cui CZ, Zhao XY (2004) The reservoir numerical simulation study with the variety of reservoir parameters. J Hydrodyn 19(3):912–915

Dou S (2005) Fine description and distribution of remaining oil in fluvial sandstone reservoirs in Beida port. China University of Geosciences, Beijing

Felsenthal M, Gangle FJ (1975) A case study of thief zones in a California waterflood. J Pet Technol 27(11):1385–1391

Jiang H (1997) Parameter determination for high permeable channels in biandong oil field by probability model. Pet Explor Dev 24:55–58

Jin YX, Lin CY (2004) Uncertainty analysis of remaining oil predicted with reservoir numerical simulation. J Univ Pet China 28(3):22–24

Jordan DW, Pryor WA (1992) Hierarchical levels of heterogeneity in a Mississippi river meander belt and application to reservoir systems. AAPG 76(10):1601–1624

Leeder MR (1973) Fluviatile fining upwards cycles and the magnitude of paleochannels. Geol Mag 110:265–276

Luchi R, Pittaluga MB, Seminara G (2012) Spatial width oscillations in meandering rivers at equilibrium. Water Resour Res 48(5):375–390

Maier F, Kocabas I (2013) Comment on "A closed-form analytical solution for thermal single-well injection-withdrawal tests" by Jung and Pruess. Water Resour Res 49(1):640–643

Sun HQ, Sun G, Wu SY (2004) Dynamic geology model establishment of reservoir parameters—taking 1~2 layer, segment 2 of Shahejie Formation, Shengtuo Oilfield, as an example. Pet Explor Dev 31:89–91

Yan B, Zhang X, Yu L et al (2014) Analysis of point dam configuration and remaining oil based on core and dense well pattern. Pet Explor Dev 41(5):597–604

Yue D, Wu S, Liu J (2007) Fine anatomy of the underground reservoir of point River dam in meandering river. Acta Petrota Sinica 28(4):99–103

Zhao H (1995) Fine development of fluvial reservoir sedimentary model by using well log pattern. In: Proceedings of the fifth international conference on petroleum engineering. International Culture Publishing Company, Beijing, SPE29963, pp 732–738

Zhou Y, Wu S, Yue D et al (2009) Analysis and identification of the factors of controlling the inclination of the inner side of the inner side of the point dam. J China Univ Pet 33(2):7–11